Modeling Transient Stresses in Spherical Vessels During Blowdown under Fire Attack

G. B. O. Falope and H. Mahgerefteh
Dept. of Chemical Engineering, University College London, London, WC1E 7JE

The development of a rigorous mathematical model for simulating the failure risk of pressurized spherical hydrocarbon containing vessels during blowdown under fire attack is described. Accounting for the important thermodynamic and interfacial mass and heat transfer processes taking place during blowdown, the model simulates the thermal and pressure stresses in the vessel wall in both the radial and tangential directions. Failure is assumed to take place when the sum of these two stresses in either direction exceeds the vessel material of construction yield strength. Application of the model to the blowdown of a condensable hydrocarbon mixture indicates that failure occurs in the vapor space due to thermal weakening of the vessel wall. Finally, the risks associated with blowdown during fire attack for a cylindrical as opposed to a spherical vessel of the same volume and prevailing conditions are compared and contrasted.

Introduction

In the oil and gas industries, large quantities of highly flammable hydrocarbons are commonly processed, stored, or transported under high pressures. These operations pose a serious safety hazard, particularly in emergency situations such as fire. In these circumstances it is essential that appropriate provisions exist to enable the safe and efficient disposal of the pressurized hydrocarbon inventory. Blowdown, or rapid emergency depressurization of the inventory to a remote storage tank or the flare stack, is the most common way of achieving this.

However, blowdown presents design and safety engineers with a dilemma. The near adiabatic expansion process results in significant cooling of the inventory, and, hence, a drop in the temperature of the inside vessel walls in contact with it (Mahgerefteh and Wong, 1999; Mahgerefteh et al., 1999, 2000, 2002). This autorefrigeration effect, on its own accord is beneficial, as it will "lessen" the effect of the fire. On the other hand, the outer vessel walls, being exposed to the thermal radiation from fire, experience a marked rise in temperature. The resulting temperature gradient along with the superimposed pressure, expose the vessel walls to considerable thermal and pressure stresses.

The preceding discussion raises an important question as to what is the optimum depressurization rate that will provide the fastest evacuation rate, while at the same time avoiding the risk of vessel rupture due to thermal and pressure stress gradients. The situation is further complicated in the case of blowdown of two-phase liquid–vapor inventories. Here, the liquid phase, having a significantly higher heat transfer coefficient than the vapor acts as an efficient heat sink. This also significantly contributes to the resulting thermal stress gradients in the vessel walls. At the same time, removal of the liquid inventory reduces the vessel's "capacity" to absorb heat, thereby resulting in a significant rise in the wall temperature. In such circumstances, the whole wisdom of removing the inventory through blowdown might be thought questionable in the first place.

Accounting for the important thermodynamic, heat, and mass transfer processes taking place during blowdown of a hydrocarbon vessel under fire attack, we recently (Mahgerefteh et al., 2001) developed a rigorous mathematical model capable of quantitatively evaluating the risk of rupture.

The application of our model to a real system revealed that, whereas during blowdown under ambient conditions, it is possible to cause brittle wall fracture due to significant cooling of the inventory, such failure under fire attack is extremely unlikely. In this case, the most likely cause of failure would be thermally induced mechanical weakening of the vessel wall in vapor space. Based on our findings, we concluded that blowdown under fire attack should be conducted as fast as practicable in order to minimize the amount of in-

Correspondence concerning this article should be addressed to H. Mahgerefteh.

ventory present in the event of vessel rupture, while at the same time deriving maximum benefit from the accompanying autorefrigeration effect.

Despite the success of our model in allowing the evaluation of the risk of vessel failure, its application was limited to cylindrical vessels. This is an important drawback, since spherical vessels are also commonly used for storage of vast amounts of pressurized hydrocarbon. For the same surface area, a spherical vessel offers a larger storage volume as compared to that for a cylindrical vessel. Furthermore, the pressure stress distribution in a spherical vessel enables better "stress containment" in comparison to a cylindrical vessel. This is due to the fact that in a cylindrical vessel, the longitudinal stresses parallel to the vessel's main axis do not contribute to maintaining the internal pressure acting on the curved surface. In contrast, in a spherical vessel, a system of equal stresses resists the internal pressure. As a result, for comparative size and wall thickness, the maximum safe working pressure for a spherical vessel is about double that for a cylindrical vessel (Popov, 1999). A spherical vessel requires an altogether different and more complex method of analysis to simulate the resultant stress distribution, and, hence, enable the evaluation of the risk of failure under fire attack.

It is noteworthy that the blowdown process under ambient conditions has been comprehensively modeled in recent years (see, for example, Haque et al., 1992a; Overa et al., 1994; Mahgerefteh and Wong, 1999). The response of pressure vessels during pressure relief under fire impingement also has been studied by a number of authors, leading to several models, such as ENGULF I (Hunt and Ramskill, 1985), ENGULF II (Ramskill, 1988), and HEATUP (Beynon et al., 1988). However, a serious drawback of these models is that apart from predicting fluid and wall temperatures, none are capable of evaluating the risk and mode of failure, as the accompanying vessel wall thermally induced stresses are not accounted for.

The TCTCM computer model (Birk, 1988) simulates the response of a long cylindrical tank exposed to an engulfing and torch-type fire. Based on comparison with field data, the model successfully predicts the tank internal pressure, the mean fluid temperatures, and wall temperature distribution. However, little detail on the formulation of the wall triaxial pressure and thermal stresses is given. Hence, the coordinate stress component responsible for rupture is unknown.

A recent detailed experimental study of the failure mechanism of vessels exposed to fire resulting in boiling liquid expanding vapor explosion (BLEVEs) has been carried out by Venart (2000). The author observes that BLEVEs result from a two-step process: the formation of an initiating tear in the dry walls of the vessel, followed by a catastrophic "unzipping" of the containment, resulting in a nearly instantaneous release of its contents. The study demonstrates that the failure mechanism ultimately leading to vessel collapse is a creep or ductile failure process.

Kielec and Birk (1997) propose a correlation to simulate the relationship between failure severity and the tank condition at failure. Scale effects on vessel failure have also been studied by Birk (1995). The models resulting from both studies are, however, limited in their scope, as both ignore the contributing effect of thermal stresses. Kielec and Birk (1997) attribute the parameters effecting rupture to the extent of deformation prior to failure and the transient-pressure history. Birk (1995), on the other hand, attributes vessel failure due to wall thinning resulting from a combination of hoop stress and high-temperature material degradation.

Other reported models are PLGS-1 and PLGS-2D (Sumathipala et al., 1992), validated by results obtained from small-scale experiments by Venart et al. (1988) and Sumathipala et al. (1988), as well as the U.K. Health and Safety Executive (Moodie et al., 1988). Both models predict loading mass, vessel internal pressure, as well as fluid and vessel wall temperature variations with time. However, neither simulates the stress distribution within the vessel wall, and, hence, does not allow the evaluation of the risk of failure and, if applicable, its mode.

Additionally, apart from those drawbacks, all of the studies reviewed are confined to cylindrical vessels.

In this article, we describe the development of a rigorous mathematical model for simulating the risk and mode of failure of spherical hydrocarbon-containing vessels during blowdown under fire attack. We apply our model to a hypothetical fire blowdown scenario to elucidate the important processes leading to vessel failure. Finally, we compare and contrast the risks associated with the blowdown during fire attack for a cylindrical as opposed to a spherical vessel of the same volume and prevailing conditions.

Model Development

In this study, failure refers to onset of inelastic deformation or yielding of vessel, resulting in buckling or some sort of permanent deformation. It is assumed to occur when the yield stress of the vessel material is exceeded. We assume a constant and uniformly distributed heat-flux representative of a pool fire engulfing the vessel. This represents a second-order nonhomogeneous boundary condition for the outside wall. The inside wall, on the other hand, dissipates energy to the adjacent fluid as dictated by the heat transfer coefficients, a third-order nonhomogeneous boundary condition.

Assuming temperature has no axial and tangential dependence, and by using the transformation for the temperature profile, $T(r,t)$, for the vessel wall as a function of distance, r, from the center of a hollow sphere at time, t,

$$U(r,t) = rT(r,t) \tag{1}$$

The subsequent mathematical formulation of the heat-conduction problem at various boundary conditions can be represented as

$$\frac{\partial^2 U}{\partial r^2} = \frac{1}{\alpha}\frac{\partial U}{\partial t} \qquad \text{in } a < r < b; \quad t = 0 \tag{2a}$$

$$-\frac{\partial U}{\partial r} + M_a U = aH_a T_f \qquad \text{at } r = a; \quad t > 0 \tag{2b}$$

$$\frac{\partial U}{\partial r} - \frac{U}{b} = bQ_f \qquad \text{at } r = b; \quad t > 0 \tag{2c}$$

$$U = rF(r) \qquad \text{at } t = 0; \quad a \le r \le b \tag{2d}$$

where

$$M_a = H_a + \frac{1}{a}, \qquad H_a = \frac{h_a}{k} \tag{3}$$

where a and b are the sphere internal and external radii, respectively, T_f is the fluid temperature adjacent to the vessel wall; h_a and k are the vessel-wall heat transfer coefficient and thermal conductivity, respectively; Q_f is the amount of impinging heat flux; α is the thermal diffusivity, and $F(r)$ is the vessel temperature profile at time zero.

Equation 1 can be separated into a steady state, $U_s(r)$, and a homogeneous, $U_h(r,t)$, problem that, upon transforming back to $T(r,t)$, yields the temperature profile for the sphere wall as

$$T(r,t) = \frac{1}{r}\left[U_s(r) + U_h(r,t)\right] \tag{4}$$

Steady-state solution

Equating time integrals to zero, the resulting steady-state solution, $U_s(r)$, can be shown to have the form

$$U_s(r) = C_1 r + C_2 \tag{5}$$

Also applying the prevailing boundary conditions (Eqs. 2b and 2c), C_1 and C_2 are given as

$$C_1 = T_a + \frac{Q_f b^2 M_a}{a H_a} \tag{6}$$

$$C_2 = -Q_f b^2 \tag{7}$$

Homogeneous solution

Equating the righthand side of Eqs. 2b and 2c to zero, the resulting homogeneous problem is solved by employing the analytical method of separation of variables (Ozisik, 1980). Assuming a separation of the form

$$U_h(r,t) = X(r)\Pi(t) \tag{8}$$

By linear superposition of the elementary solutions of the space and time variables, $X(r)$ and $\Pi(t)$, respectively, Eq. 8 is given by

$$U_h(r,t) = \sum_{m=1}^{\infty} c_m X(\beta_m,r) e^{-\alpha\beta_m^2 t} \tag{9}$$

where the eigenfunctions $X(\beta_m,r)$ and $e^{-\alpha\beta_m^2 t}$ are the elementary solutions for the space and time variables, respectively. The superposition coefficient, c_m, is obtained by applying the initial condition to Eq. 9 and by making use of the orthogonality of the eigenfunctions to give

$$c_m = \frac{1}{N(\beta_m)} \int_{r=a}^{r=b} X(\beta_m,r) F(r)\, dr \tag{10}$$

Substitution of c_m from the preceding equation into Eq. 9 gives the transformed homogeneous temperature profile for the sphere as

$$U_h(r,t) = \sum_{m=1}^{\infty} \frac{1}{N(\beta_m)} X(\beta_m,r) e^{-\alpha\beta_m^2 t} \int_{r=a}^{r=b} X(\beta_m,r') F(r')\, dr' \tag{11}$$

where the norm $N(\beta_m)$ and eigenfunctions $X(\beta_m,r)$ are given by

$$\frac{1}{N(\beta_m)} = 2\left[\left(\beta_m^2 + M_a^2\right)\left[(b-a) - \frac{1}{b\left(\beta_m^2 + \left(\frac{1}{b}\right)^2\right)}\right] + M_a\right]^{-1} \tag{12}$$

and

$$X(\beta_m,r) = \beta_m \cos\beta_m(r-a) + M_a \sin\beta_m(r-a) \tag{13}$$

The eigenvalues are the positive roots of the transcendental equation given by

$$\tan\beta_m(b-a) = \frac{\beta_m\left(M_a - \frac{1}{b}\right)}{\beta_m^2 + \frac{M_a}{b}} \tag{14}$$

Equations 12 and 13 are then substituted into Eq. 11 to give the vessel wall radial-temperature profile.

Thermal and pressure stresses

The radial and tangential thermal stresses (longitudinal stresses are nonexistent) for a hollow spherical vessel are, respectively, given by (Timoshenko and Goodier, 1987)

$$\sigma_\theta^t = \frac{\tau E}{(1-\mu)r^3}\left[\frac{2r^3 + a^3}{b^3 - a^3}\int_a^b Tr^2\, dr + \int_a^r Tr^2\, dr - Tr^3\right] \tag{15a}$$

$$\sigma_R^t = \frac{2\tau E}{(1-\mu)r^3}\left[\frac{r^3 - a^3}{b^3 - a^3}\int_a^b Tr^2\, dr - \int_a^r Tr^2\, dr\right] \tag{15b}$$

where τ is the coefficient of thermal expansion, E is the modulus of elasticity, μ is Poisson's ratio, and T is the temperature profile.

The pressure stresses in a thick-walled spherical vessel are obtained by employing a characteristic method of the mathematical theory of elasticity as presented by Nichols (1971). This is achieved by relating the balance of forces within a section of vessel wall to the geometrical relations of deformation using the generalized Hooke's law, with the resulting differential equation solved subject to the prescribed boundary

conditions. The resulting tangential and radial pressure stresses are, respectively, given by

$$\sigma_\theta^p = A_1\left(1+\frac{b^3}{2r^3}\right) - A_2\left(1+\frac{a^3}{2r^3}\right) \tag{16a}$$

$$\sigma_R^p = A_1\left(1-\frac{b^3}{r^3}\right) - A_2\left(1-\frac{a^3}{r^3}\right) \tag{16b}$$

where

$$A_1 = \frac{P_a}{R^3-1}, \qquad A_2 = \frac{P_b R^3}{R^3-1} \qquad \text{and} \qquad R = \frac{b}{a} \tag{17}$$

Here P_a and P_b are the inside and outside (ambient) pressures, respectively.

The total radial and tangential stresses at any point across the vessel wall thickness are obtained by adding the pressure and thermal stresses obtained from Eqs. 15 and 16 just given. A comparison between the resulting total stresses and the vessel's material of construction yield stress at the prevailing temperature enables the evaluation of the risk of vessel failure.

Heat transfer, thermodynamics, and fluid flow

Forced and natural convection have been shown to govern the heat transfer mode in the vapor phase during blowdown (Haque et al., 1992b; Overa et al., 1994; Moodie et al., 1988). In this study, we employ Petukhov and Popov's (Perry and Green, 1997) correlation, with the fanning factor determined by an equation recommended by Filonenko (Perry and Green, 1997) to account for forced convection. McAdam's correlation (Incropera and DeWitt, 1996) is used to obtain the convective heat transfer coefficient for the section of the vessel exposed to vapor for both heat transfer surfaces facing either up or down. This correlation approximates the curvature of the vessel wall by assuming it as a plane with the same surface area.

When the liquid volume drops below half the volume of the vessel, the correlation for the "transfer surface facing up" is used to determine the heat transfer coefficient of the unwetted section below the vessel center line. The radiative heat transfer due to the relatively high wall temperatures (>300°C) experienced in the dry walls (Moodie et al., 1988) is accounted for by using standard correlations (see, for example, Incropera and DeWitt, 1996).

Heat transfer between the vessel wall and the liquid phase is governed by boiling heat transfer, as determined by the excess temperature. Under fire conditions, nucleate, transition, and stable-film boiling heat transfer can exist. In this study, however, the excess temperatures reached are in the range of nucleate boiling only. This is consistent with experiments by Moodie et al. (1985) showing that the critical heat flux beyond which transition boiling begins is not reached. We use Rosenhow's correlation (Incropera and DeWitt, 1996) to account for nucleate boiling.

The amount of heat transferred to either fluid phase is determined by using an iterative procedure (NAG Fortran Library, 1999). This involves making an initial guess of the unknown inner-wall temperature, $T_{a,i}(t)$, at time, t, and then obtaining the corresponding heat transfer coefficient, $h(T_{a,i}(t))$, by use of the appropriate correlation for either the wetted- or unwetted-wall surface. The radial temperature profile can then be obtained from Eq. 11 to give a new value for the inside wall temperature, $T_{a,i+1}(t)$. Convergence is achieved when

$$T_{a,i+1}(t) - T_{a,i} \le 10^{-3} \tag{18}$$

The fluid/wall heat transfer to either of the phases is then obtained from

$$Q = h|T_a(t) - T_f|A\Delta t \tag{19}$$

where A is the heat transfer area, and $T_a(t)$ is the solution temperature.

During the numerical solution of the blowdown process, the initial temperature profile, $F(r)$, in Eq. 16 needs to be determined at every step. This is achieved by the use of a curve-fitting algorithm (NAG Fortran Library, 1999) to represent the radial temperature profile of the preceding numerical step as a polynomial function and transferring to the subsequent step.

Reducing pressure steps is used to numerically simulate the depressurization process, with the fluid temperature adjacent to the wall determined from pressure–entropy flash calculations. Full details of the pertinent model are given elsewhere (Mahgerefteh and Wong, 1999), and, hence, only a brief account is given here. In essence, the model accounts for all the important processes taking place during blowdown, including interfacial heat and mass transfer, as well as nonequilibrium effects between the constituent phases. Its performance during blowdown under ambient conditions has been fully validated against experimental data.

The new pressure interval, ΔP_i, is obtained from the previous pressure interval, ΔP_{i-1}, via

$$\Delta P_i = \Delta P_{i-1} \times r \tag{20}$$

where r is the pressure ratio.

The corresponding entropy is given by

$$S_i = S_{i-1} + \frac{Q}{T_f} \tag{21}$$

where Q is the amount of heat transfer into either the vapor or liquid phases.

Thermodynamic and phase equilibrium properties are determined using the Peng–Robinson (Peng and Robinson, 1976) equation of state. This equation has been shown to be particularly applicable to high-pressure hydrocarbon mixtures (deReuck et al., 1996; Assael et al., 1996). The number of phases present at any given time is determined using the Gibbs tangent-plane stability test (Michelsen, 1982). The nonisentropic expansion of each fluid phase during blowdown is accounted for by assuming a polytropic expansion process (Bett et al., 1975) in which both heat and work are considered. The fluid approaching the blowdown valve can be either single or two phase. The procedure for determining the discharge rate and the state of the fluid phase at the orifice is described elsewhere (Haque et al., 1992a; Mahgerefteh and Wong, 1999). In essence, it is based on carrying out an energy balance across the orifice, assuming isen-

tropic expansion coupled with thermodynamic and phase equilibrium.

Based on experimental observations for low liquid fill levels (Moodie et al., 1988), we assume that both vapor and liquid are well mixed, ignoring temperature stratification within each constituent phase. Furthermore, pressure is assumed to be spatially uniform within the vessel.

Results and Discussion

The following describes the results of the application of our model to a hypothetical case involving the blowdown of a spherical vessel containing a hydrocarbon mixture under fire attack from a pool fire (90 kW/m^2). For the sake of comparison, the vessel volume (3.02 m^3), wall thickness (0.059 m), and inventory composition (mole %: C_1; 64%, C_2; 6%, n-C_3; 28% and n-C_4; 2%) are taken to be the same as those for the blowdown of a cylindrical vessel simulated in our previous study (Mahgerefteh et al., 2002). The prevailing temperature and pressure are taken as 293 K and 116 bara, respectively. Under these conditions, the hydrocarbon inventory is in the gaseous state, although depressurization results in the rapid formation of a two-phase mixture followed by its evaporation as heat transfer from the heated wall takes place.

It is noted that the condensation of the vapor following its expansion may result in a mist protecting the vessel's interior. However, it is assumed that this thin film will rapidly evaporate following the transfer of heat from the fire, and, thus, have a negligible effect on the vessel's heat transfer characteristics. The vessel is assumed to be made of carbon steel alloy (BS 3100 AM1) discharging through 0.01-m-diam. orifice, with a discharge coefficient of 0.8.

Temperature profiles

Figure 1 shows the variations of unwetted (vapor space) outside wall (curve A), inside wall (curve B), and bulk vapor (curve C) temperatures as a function of time during blowdown under fire attack. The corresponding data for the wetted section of the vessel walls and bulk liquid are given in Figure 2. The state of the fluid within the vessel during blowdown is indicated in Figure 1.

As it may be observed from Figure 1, the vapor temperature (curve C) remains relatively unchanged during the first 850 s of blowdown, following which it rapidly increases to a maximum value of about 1,000 K upon the completion of blowdown. The rapid transition in the temperature is due to the fact that most of the heat transferred from the vessel walls to the fluid in the first 850 s of blowdown is expended as latent heat of vaporization for the two-phase mixture. Further application of heat beyond this time domain simply results in the formation of superheated vapor and a subsequent significant rise in the vapor temperature. It is noteworthy that the temperature difference across the vessel wall remains rel-

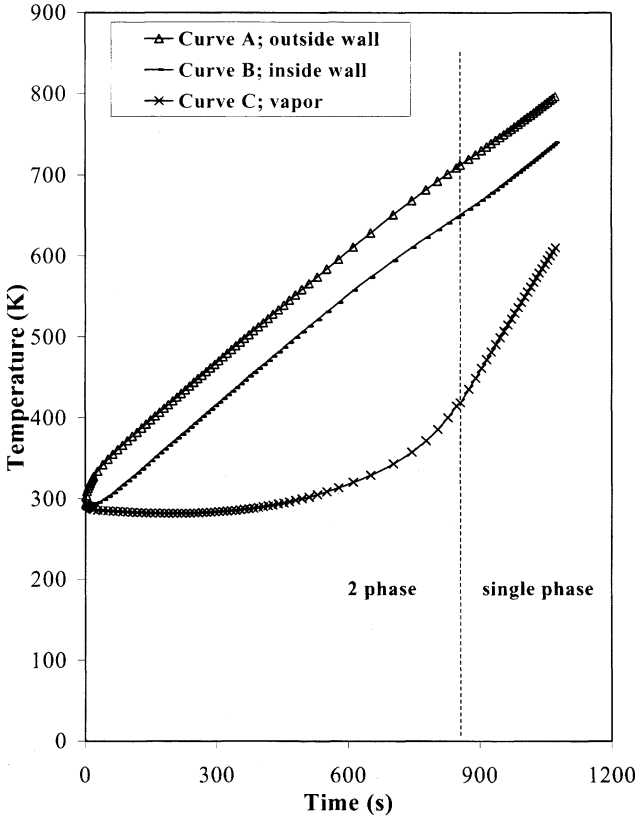

Figure 1. Unwetted vessel wall and bulk vapor temperature/time response during blowdown under fire attack.

The fluid state within the vessel at any time during depressurization is indicated.

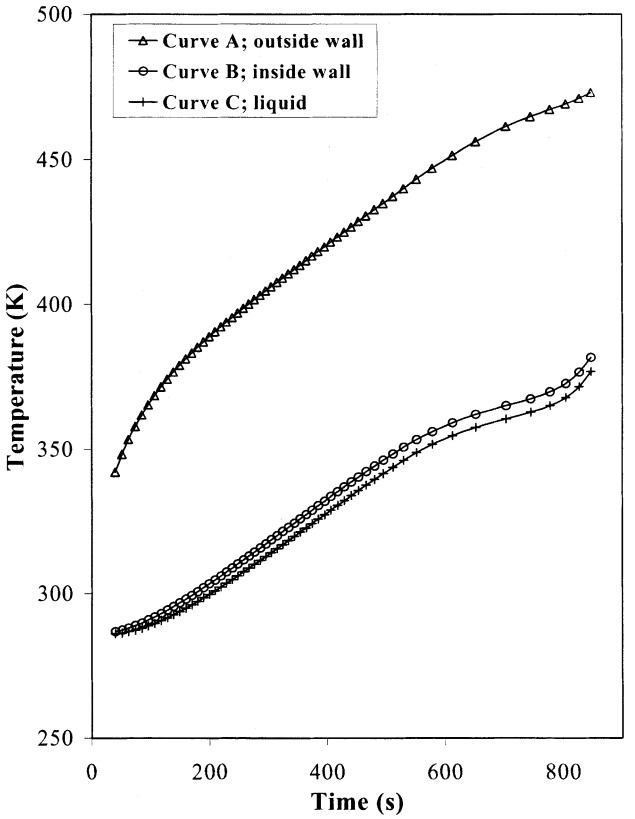

Figure 2. Wetted vessel wall and bulk vapor temperature/time response during blowdown under fire attack.

atively small and constant at ca. 50 K throughout the depressurisation process. Referring to Figure 2, the corresponding temperature difference in the wetted wall is significantly higher at 100 K. This is because of the higher heat transfer coefficient in the wetted section, which also results in the inside wetted-wall temperature being very close to that of the liquid inventory in contact with it.

The significantly lower bulk liquid temperature (Figure 2, curve C) as opposed to the vapor temperature (Figure 1, curve C) is a consequence of the fact that the former acts as a far better "heat sink" due to its much higher heat capacity. The preceding is manifested in the unwetted-wall temperature being some 500 K hotter than that of the wetted wall.

Finally, the data for the liquid phase cease at ca. 850 s (Figure 2), since this marks the complete transformation of the two-phase mixture into vapor.

If, when, and where rupture occurs depends on the relative importance of the higher temperature gradients (and, hence, thermal stresses) in the wetted section as opposed to the thermal weakening of the vessel wall in the vapor space due to the elevated temperatures. The preceding requires detailed analysis of the accompanying thermal- and pressure-stress profiles within the vessel walls.

Stress profiles

Figure 3a and 3b, respectively, show the variations of the total (thermal and pressure) normalized radial- and tangential-stress profiles for the unwetted vessel wall as a function of time during blowdown under fire attack. Figure 4a and 4b, on the other hand, show the corresponding data for the wetted-wall section. The various stress profiles have been normalized with respect to the vessel material of construction's yield stress (Brandes, 1983) at the prevailing vessel integral temperature, $\Psi(K)$. This is given by

$$\Psi(K) = \frac{\int_a^b T(r,t)}{b-a} \tag{22}$$

Normalized total stress values greater than unity indicate imminent vessel failure. Positive and negative values, on the other hand, represent tensile and compressive stresses, respectively. Table 1 shows the appropriate temperature/yield stress data (Brandes, 1983).

Returning to Figures 3a and 4a, it is clear that the total normalized radial stresses are insignificant, and, hence, pose no threat to vessel mechanical integrity. These stresses are relatively small, because radial pressure stresses are compressive, while the corresponding radial thermal stresses, although of similar magnitude, are tensile, thus to a large extent, they counteract each other's effect.

As expected, the total radial stresses are zero on the outer surface of the vessel wall, while on the inside wall, the pressure stress is maximum but the thermal stress is zero. Also, for both the wetted and unwetted walls, the radial stresses

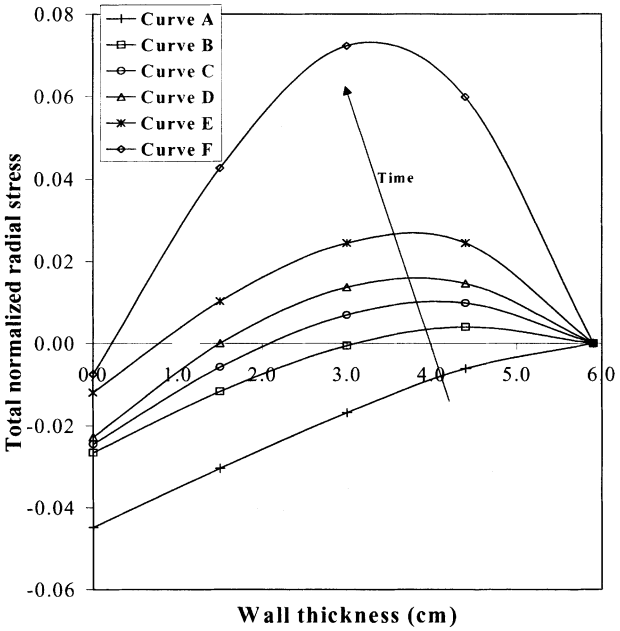

Figure 3a. Unwetted wall normalized total radial stress profiles at different times during blowdown under fire attack.

(Curve A: 10 s, Ψ = 298.3 K; Curve B: 296 s, Ψ = 432.5 K; Curve C: 612 s, Ψ = 576.8 K; Curve D: 904 s, Ψ = 693.6 K; Curve E: 1201 s, Ψ = 817.9 K; Curve F: 1500, Ψ = 956.1 K).

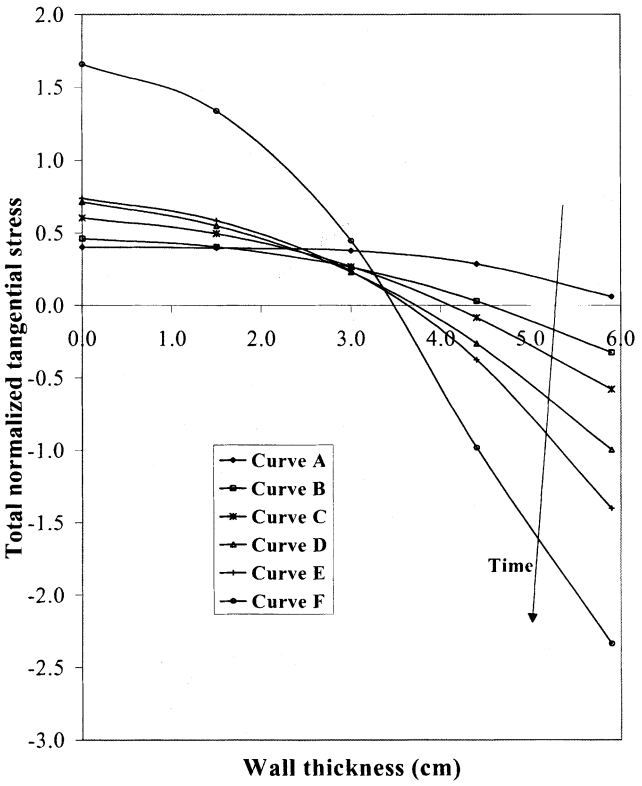

Figure 3b. Unwetted wall normalized total tangential stress profiles at different times during blowdown under fire attack.

(Curve A: 10 s, Ψ = 298.3 K; Curve B: 296 s, Ψ = 432.5 K; Curve C: 612 s, Ψ = 576.8 K; Curve D: 1072 s, Ψ = 693.6 K; Curve E: 1201 s, Ψ = 817.9 K; Curve F: 1500, Ψ = 956.1 K).

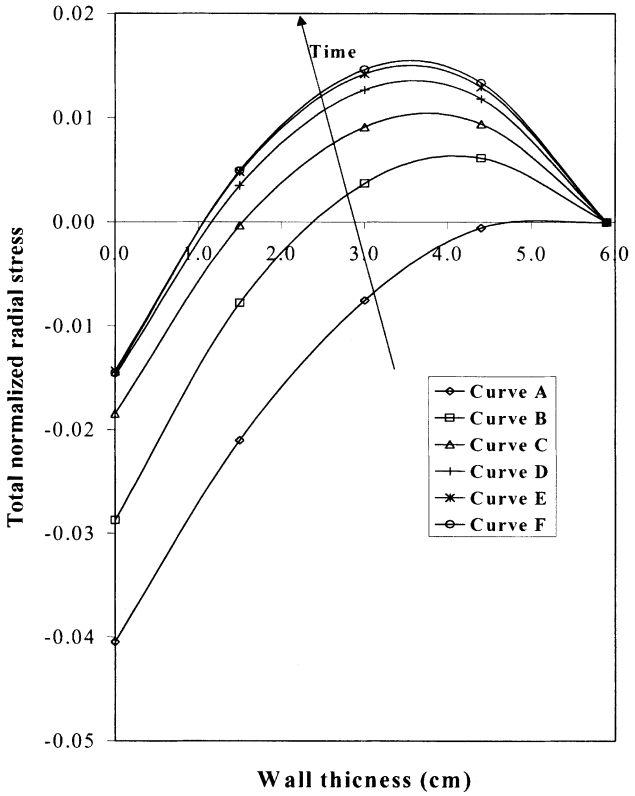

Figure 4a. Wetted wall normalized total radial stress profiles at different times during blowdown under fire attack.

(Curve A: 40 s, Ψ = 309.5 K; Curve B: 200 s, Ψ = 344.2 K; Curve C: 406 s, Ψ = 376.0 K; Curve D: 612 s, Ψ = 404.5 K; Curve E: 704 s, Ψ = 413.0 K; Curve F: 805 s, Ψ = 426.2 K).

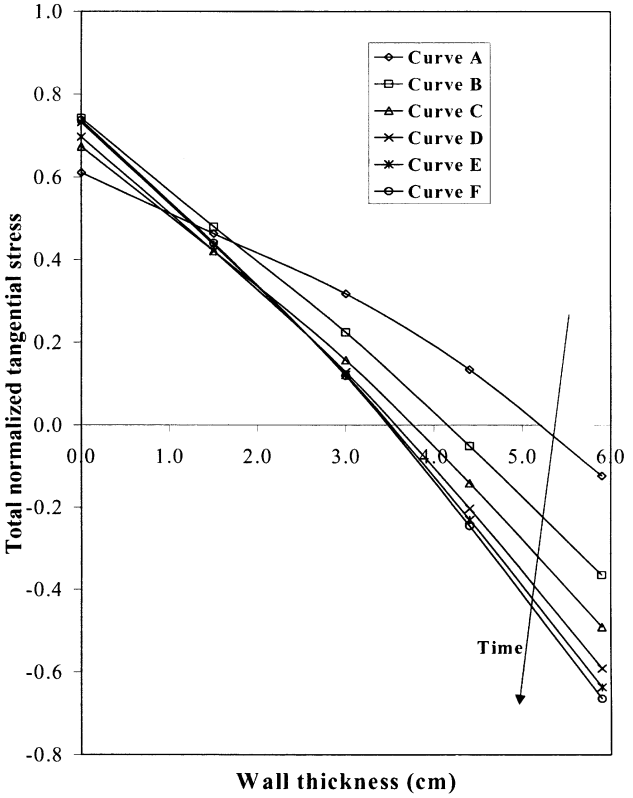

Figure 4b. Wetted wall normalized total tangential stress profiles at different times during blowdown under fire attack.

(Curve A: 40 s, Ψ = 309.5 K; Curve B: 200 s, Ψ = 344.2 K; Curve C: 406 s, Ψ = 376.0 K; Curve D: 612 s, Ψ = 404.5 K; Curve E: 704 s, Ψ = 413.0 K; Curve F: 805, Ψ = 426.2 K).

(Figures 3a and 4a) change from purely compressive stresses at the start of blowdown to predominantly tensile stresses as time proceeds. This is due to the fact that at the beginning of blowdown, the compressive pressure stresses are at their peak with little thermal tensile stress contribution from the impinging fire. With the passage of time, these two effects reverse roles, and, hence, the observed increase in the total tensile stresses.

Referring to the tangential stress profiles (Figures 3b and 4b), several important trends in the data can be observed. These are:

(1) At any given time following blowdown, the total normalized tangential stresses are greater in the dry (Figure 3b), as opposed to the wet, vessel walls (Figure 4b). This is a consequence of the greater ability of the liquid to absorb thermal energy, in turn manifested in the observed significantly lower wetted vessel wall integral temperatures, as compared to the dry wall.

(2) The complete transformation of the liquid inventory into vapor at approximately 856 s during blowdown is marked by a rapid increase in the total normalized tangential stress in the vapor phase (Figure 3b, curves D–F).

(3) Failure occurs by compressive shear near the vessel's outer unwetted wall some 1,070 s following blowdown (Figure 3b, curve E). This is primarily a consequence of the thermal weakening of the vessel wall material. Although the wetted wall is exposed to a larger thermal stress gradient, the significantly higher unwetted wall temperature results in a reduction in its yeild stress and the vessels ultimate failure.

Pressure and inventory/time profiles: Comparison with a cylindrical vessel

Figures 5 and 6 show the variations of pressure and inventory with time following blowdown under fire attack for the spherical vessel (curves A) until the time of vessel failure due to thermal yielding. The corresponding data for the blowdown of the cylindrical vessel (curves B) of the same volume and prevailing conditions under fire attack (Mahgerefteh et al., 2001) are also given for comparison.

Table 1. Yield Stress Data for Carbon Steel BS3100 AM1

Temp. (°C)	Yield Stress (MPa)
Room Temp.	235
100	187
200	187
300	131
400	137
500	97

Note: Composition: 14% C, 29% Si, 45% Mn; annealed (Brandes, 1983).

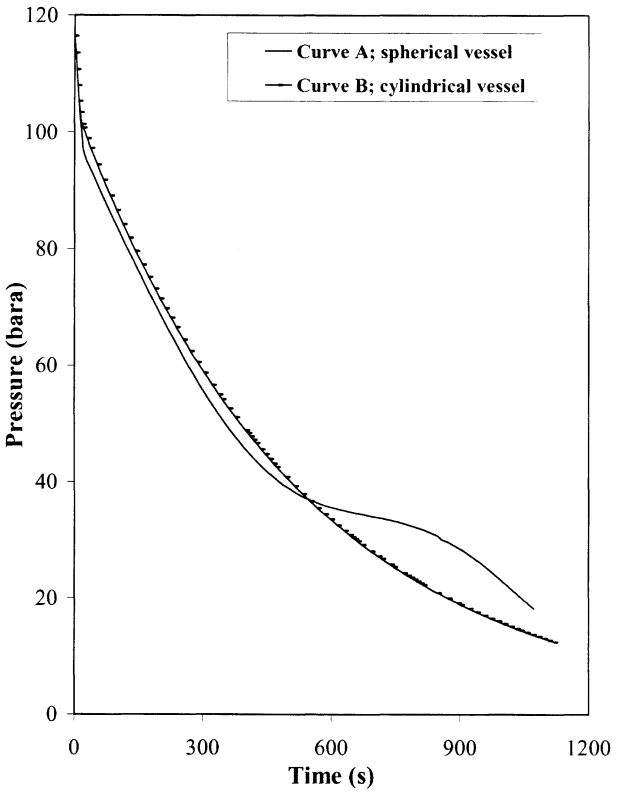

Figure 5. Pressure variation with time during blowdown under fire attack.

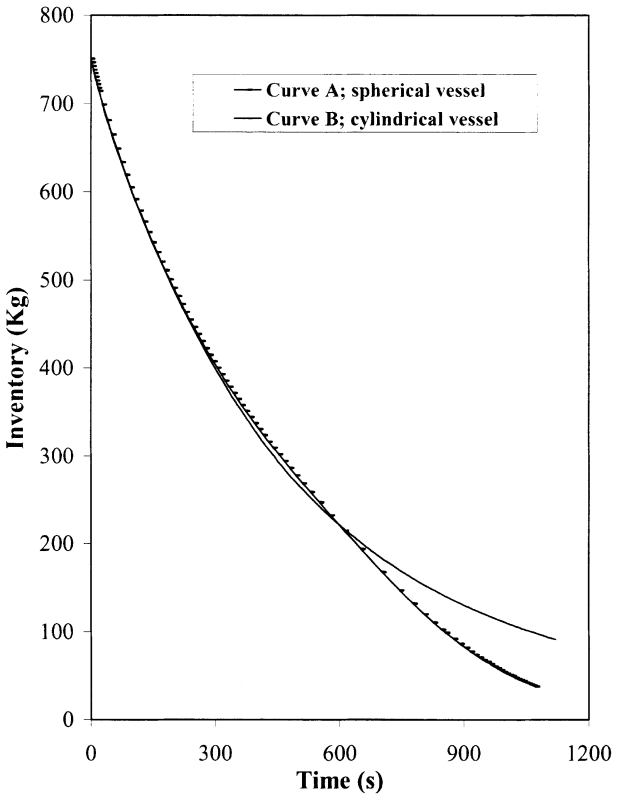

Figure 6. Inventory variation with time during blowdown under fire attack.

Referring to Figure 5, in the case of the spherical vessel (curve A), the complete flashing of the two-phase inventory is marked by an inflection point in the pressure curve between 600 s and 900 s following blowdown. This effect is not observed in the case of the cylindrical vessel (curve A), since the inventory remains in the two-phase region throughout the discharge process. The difference in the fluid-state behavior is primarily a consequence of the greater wall heat transfer area available in the case of the spherical vessel. It is also manifested in a faster rate of loss in inventory during the latter part of the blowdown process (cf. curve A and curve B, Figure 6).

Table 2 is a summary of the main differences in behavior between the two vessels during blowdown under fire attack. Referring to the table, it is clear that both vessels behave in a similar manner in response to fire attack. The marginally shorter (ca. 50 s) failure time in the case of the spherical vessel is due to the larger heat transfer area available, which results in a faster evaporation rate of the two-phase mixture. As compared to the cylindrical vessel, this is manifested in approximately 50 kg less inventory being potentially available to feed the fire at the time of failure.

Conclusion

In this article the development of a rigorous mathematical model for predicting the transient thermal and mechanical behavior of spherical vessels during blowdown under fire attack are described. The study was initiated because of the extensive use of spherical vessels for the storage of large quantities of highly flammable pressurized hydrocarbons. It complements our previous work on the modeling of the behavior of the cylindrical vessels, which are also used, although less extensively, for the storage of hydrocarbons. For

Table 2. Behavior of spherical vs. cylindrical vessels during blowdown under fire attack.

	Spherical Vessel	Cylindrical Vessel
Time of failure following blowdown(s)	1070	1120
Failure mode	Tangential shear in the vapor space	Tangential shear in the vapor space
Vessel pressure at time of failure (bara)	18.10	12.90
Inventory remaining in vessel at time of failure (kg)	37.5	91.2

such vessels, the longitudinal stresses parallel to the main axis do not contribute to maintaining the internal pressure acting on the curved surface. In contrast, in a spherical vessel, a system of equal stresses resists the internal pressure. As a result, a spherical vessel requires an altogether different and more complex method of analysis to simulate the resultant stress distribution, and, hence, enable the evaluation of the risk of failure under fire attack.

The model described accounts for all the important processes taking place during blowdown, including nonequilibrium effects between the constituent phases, and the interfacial heat and mass transfer processes. The risk of failure is ascertained by comparing the sum of the transient vessel-wall thermal and pressure stresses in the radial and tangential planes with its material-of-construction yield strength at the prevailing conditions.

Application of our model to the hypothetical blowdown scenario of a condensable hydrocarbon gas mixture under fire attack reveals an intriguing and complex interaction of a number of processes that ultimately undermine the vessels mechanical integrity. The prevailing physical state of the pressurized inventory plays a fundamental role in the unfolding of the sequence of events.

In the case of a gaseous hydrocarbon inventory, we find that depressurization leads to rapid condensation into a two-phase mixture in the first few seconds following blowdown. This results in two distinct and competing thermal behaviors in the wetted and unwetted sections of the storage vessel.

In the wetted section, the superior ability of the liquid inventory to absorb heat from the impinging fire results in relatively low vessel inside-wall temperatures. This is, however, at the expense of exposing the vessel wall to high thermal stresses due to the large temperature gradients. The resulting thermal stresses, accompanied by the superimposed pressure stresses, could, in their own right, cause vessel failure.

The state of affairs in the unwetted section of the vessel is somewhat different. Here, the vapor being a poor conductor of heat leads to the inside wall approaching the high outside wall temperature. Although this reduces the thermal stresses, the elevated "average" metal temperature results in the mechanical weakening of the vessel wall due to a reduction in its yield strength. The preceding result, accompanied by the superimposed pressure stress, also poses a threat to the vessel's mechanical integrity.

As blowdown proceeds, the inevitable vaporization of the two-phase mixture results in the dominance of the heat transfer effects in the vapor space. Our case study indicates that failure occurs in the unwetted section of the vessel because of tangential compressive stresses some 1070 s after blowdown.

It should be pointed out that in this study, for the sake of simplification, we have ignored the wall pressure and thermal stresses of the liquid/vapor interface, as well as temperature stratification effects. These will be the subject of a future study.

A comparison of the behavior of a cylindrical vessel with the same volume, wall thickness, and prevailing conditions as the spherical vessel reveal small differences in response during blowdown under fire attack. The observed slightly shorter time to reach failure in the case of the spherical vessel is attributed to its larger wall heat transfer area, which ultimately leads to the complete evaporation of the two-phase inventory. As a consequence, the amount of inventory present at the time of failure is smaller than that in the cylindrical vessel. In the latter case, the inventory remains in the two-phase region throughout the blowdown process.

Notation

A = area
a = vessel inside radius
b = vessel outside radius
E = modulus of elasticity
h_a = inside-wall heat-transfer coefficient
k = thermal conductivity
$N(\beta_m)$ = normalized integral (norm)
P = pressure
Q = heat input to fluid
Q_f = external heat flux (fire)
r = radius
S = entropy
t = time duration
T = temperature
T_a = inside wall temperature
T_f = fluid temperature
$U_S(r)$ = transformed steady-state temperature profile
$U_h(r,t)$ = transformed homogeneous temperature profile
$X(\beta_m,r)$ = eigenfunction

Greek letters

α = thermal diffusivity
β_m = eigenvalue
ψ = integral wall temperature
τ = coefficient of thermal expansion
μ = Poisson's ratio
σ_θ^t = tangential thermal stress
σ_r^t = radial thermal stress
σ_θ^P = tangential-pressure stress
σ_r^P = radial-pressure stress

Literature Cited

Assael, M. J., J. P. Martin Trusler, and T. Tsolakis, *Thermophysical Properties of Fluids*, Imperial College Press, London (1996).

Bett, K. E., J. S. Rowlinson, and G. Saville, *Thermodynamics for Chemical Engineers*, Athlone, London (1975).

Beynon, G. V., L. T. Cowley, L. M. Small, and I. Williams, "Fire Engulfment of LPG Tanks: HEATUP, A Predictive Model," *J. of Hazard. Mater.*, **20**, 227 (1988).

Birk, A. M., "Modelling the Response of Tankers to External Fire Impingement," *J. Hazard. Mater.*, **20**, 197 (1988).

Birk, A. M., "Scale Effects of Fire Exposure of Pressure-Liquefied Gas Tanks," *J. Loss Prev. Process Ind.*, **8**, 275 (1995).

Brandes, E. A., ed., *Smithells Metals Reference Book*, Butterworths, London (1983).

DeReuck, K. M., R. J. B. Craven, and A. E. Elhassan, *Transport Properties of Fluids: Their Correlation, Prediction and Estimation*, J. Millat, J. H. Dymond, and C. A. Nieto de Castro, eds., IUPAC, Cambridge Univ. Press, Cambridge (1996).

Haque, M. A., S. M. Richardson, and G. Saville, "Blowdown of Pressure Vessels. I. Computer Model," *Trans. Inst. Chem. Eng., Part B: Process Saf. Environ. Prot.*, **70**(B1), 1 (1992a).

Haque, M. A., S. M. Richardson, G. Saville, G. Chamberlain, and L. Shirvill, "Blowdown of Pressure Vessels. II. Experimental Validation of Computer Model and Case Studies," *Trans. Inst. Chem. Eng., Part B: Process Saf. Environ. Prot.*, **70**(B1), 10 (1992b).

Hunt, D. L. M., and P. K. Ramskill, "The Behavior of Tanks Engulfed in Fire—The Development of a Computer Program," Inst. Chem. Eng. Symp. on The Assessment and Control of Major Hazards, Birmingham, U.K. (1985).

Incropera, F. P., and D. P. DeWitt, *Fundamentals of Heat and Mass Transfer*, 4th Ed., Wiley, New York (1996).

Kielec, D. J., and A. M. Birk, "Analysis of Fire-Induced Ruptures of 400-L Propane Tanks," *J. Pres. Vessel Technol.*, **119**, 365 (1997).
Mahgerefteh, H., P. Saha, and I. G. Economou, "A Study of the Dynamic Response of Emergency Shut-down Valves Following Full Bore Rupture of Long Pipelines," *Trans. I. Chem. E.: Process Safety and Environmental Protection*, **75**(B4), 201 (1997).
Mahgerefteh, H., and S. M. A. Wong, "A Numerical Blowdown Simulation Incorporating Cubic Equations of State," *Comput. Chem. Eng.*, **23**(9), 1309 (1999).
Mahgerefteh, H., P. Saha, and I. G. Economou, "Fast Numerical Simulation for Full Bore Rupture of Pressurized Pipelines," *AIChE J.*, **45**(6), 1191 (1999).
Mahgerefteh, H., P. Saha, and I. G. Economou, "Modeling Fluid Phase Transition Effects on the Dynamic Behavior of ESDV," *AIChE J.*, **46**(5), 997 (2000).
Mahgerefteh, H., G. B. O. Falope, and A. O. Oke, "Modeling Blowdown of Cylindrical Vessels Under Fire Attack," *AIChE J.*, **48**, 401 (2002).
Michelsen, M. L., "The Isothermal Flash Problem: I. Stability," *Fluid Phase Equilib.*, **9**, 1 (1982).
Moodie, K., K. Billinge, and D. P. Cutler, "The Fire Engulfment of LPG Storage Tanks," *Inst. Chem. Eng. Symp. Ser. No. 193*, Rugby, U.K., p. 87 (1985).
Moodie, K., L. T. Cowley, R. B. Denny, L. M. Small, and I. Williams, "Fire Engulfment Tests on a 5 tonne LPG Tank," *J. Hazard. Mater.*, **20**, 55 (1988).
NAG Fortran Library, Mark 16, *The Numerical Algorithms Group Limited*, Oxford, UK (1999).
Nichols, J., ed., *Pressure Vessels Design*, Butterworths, London (1971).
Overa, S. J., E. Stange, and P. Salater, "Depressurization of Temperatures and Flare Rates During Depressurisation and Fire," *Proc. GPA Annual Convention*, Aberdeen, U.K., p. 235 (1994).
Ozisik, M. N., *Heat Conduction*, Wiley, New York (1980).
Peng, D. Y., and D. B. Robinson, "A New Two-Constant Equation of State," *Ind. Eng. Chem. Fundam.*, **15**, 59 (1976).
Perry, R. H., and D. W. Green, *Perry's Chemical Engineering Handbook*, 7th Ed., McGraw Hill, London (1997).
Popov, E. P., *Engineering Mechanics of Solids*, Prentice Hall, Upper Saddle River, NJ (1999).
Ramskill, P. K., "A Description of the 'ENGULF' Computer Codes —Codes to Model the Thermal Response of an LPG Tank either Fully or Partially Engulfed by Fire," *J. Hazard. Mater.*, **20**, 177 (1988).
Sumathipala, U. K., F. R. Steward, and J. E. S. Venart, "The Experimental Thermohydraulics of Small Break Loss of Coolant Accidents," *Proc. Int. ENS/ANS Conf. on Thermal Reactor Safety (NUCSAFE"88)*, New Brunswick, Canada, p. 1103 (1988).
Sumathipala, U. K., G. V. Hadjisophocleous, N. U. Aydemir, C. M. Yu, A. C. M. Sousa, F. R. Steward, and J. E. S. Venart, "Fire Engulfment of Pressure-Liquefied Gas Tanks: Experiments and Modeling," *Fire Hazard Fire Risk Assess.*, ASTM STP, **1150**, 100 (1992).
Timoshenko, S. P., and J. N. Goodier, *Theory of Elasticity*, McGraw-Hill, New York (1987).
Venart, J. E. S., U. K. Sumathipala, F. R. Steward, and A. C. M. Sousa, "Experiments on the Thermohydraulic Response of Pressure Liquefied Gases in Externally Heated Tanks with Pressure Relief," *Plant Oper. Prog.*, **7**, 139 (1988).
Venart, J. E. S., "Boiling Liquid Expanding Vapor Explosions (BLEVEs): A Reexamination of the Causes and Consequences," *Proc. Soc. Loss Prev. Oil, Chem. Process Ind.*, **5**, 1109 (2000).

Manuscript received Oct. 1, 2001, revision received Sept. 6, 2002, and final revision received Dec. 18, 2002.